AD-A135 813 CARS STUDIES OF NITRAMINE LOVA PROPELLANT COMBUSTION 1/1
(U) GEO-CENTERS INC NEWTON UPPER FALLS MA
K ARON ET AL. NOV 83 ARLCD-TR-83045 DAAK10-81-C-0266
UNCLASSIFIED F/G 19/1 NL

END
DATE FILMED
1-84
DTIC

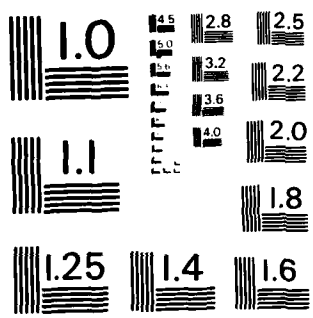

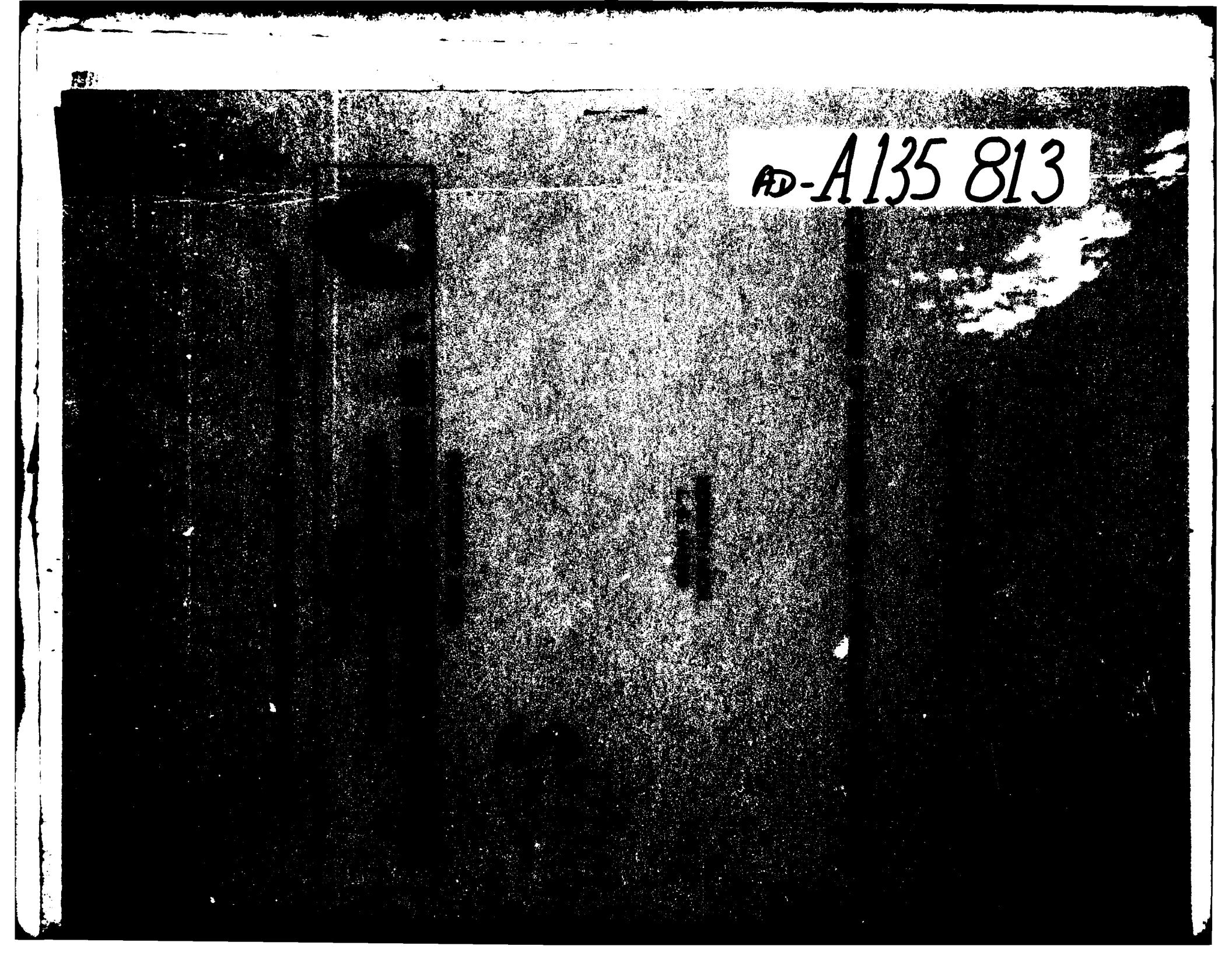
AD-A135 813

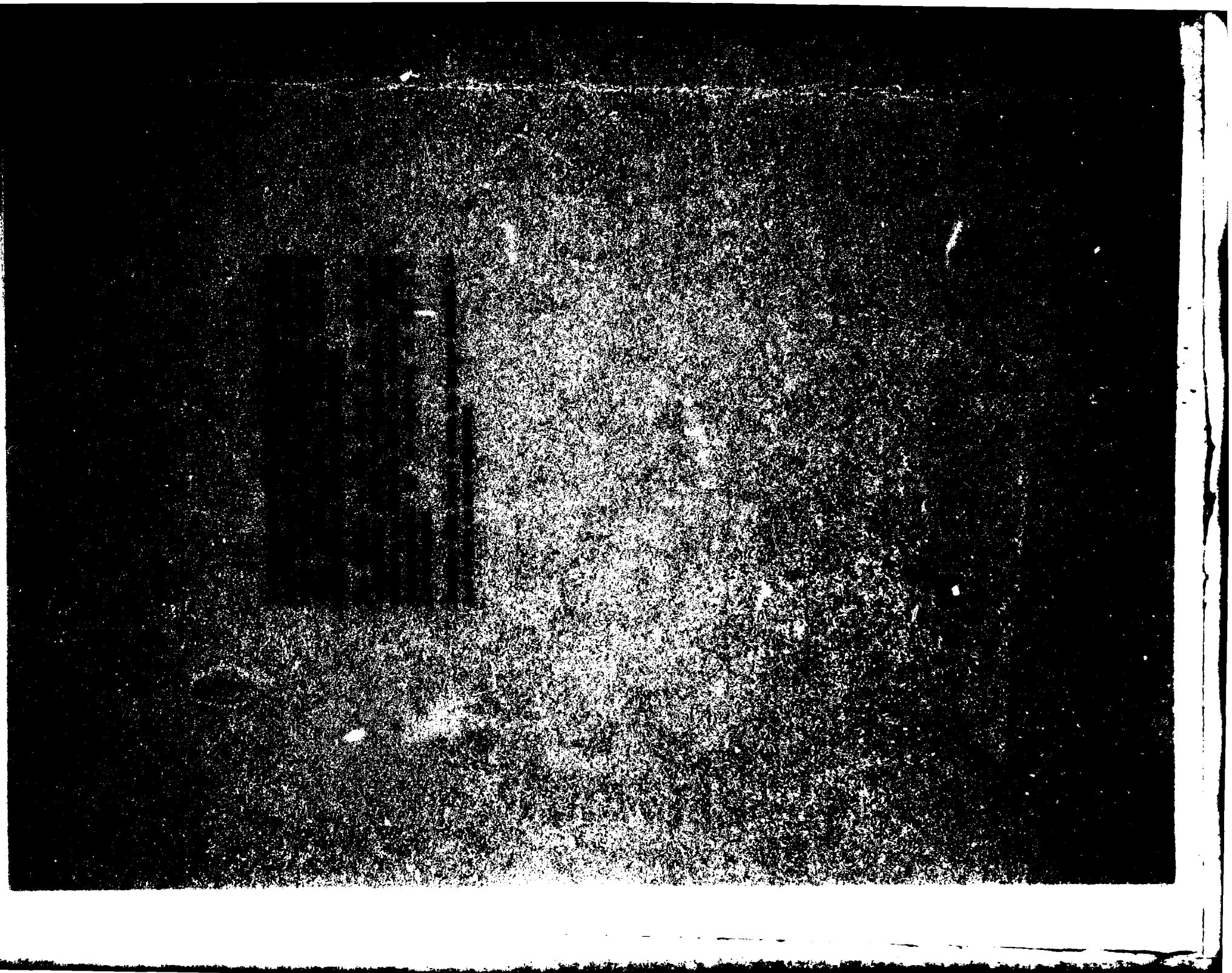

UNCLASSIFIED

SECURITY CLASSIFICATION OF THIS PAGE (When Data Entered)

REPORT DOCUMENTATION PAGE		READ INSTRUCTIONS BEFORE COMPLETING FORM
1. REPORT NUMBER Technical Report ARLCD-TR-83045	2. GOVT ACCESSION NO. AD-A135 813	3. RECIPIENT'S CATALOG NUMBER
4. TITLE (and Subtitle) CARS STUDIES OF NITRAMINE LOVA PROPELLANT COMBUSTION		5. TYPE OF REPORT & PERIOD COVERED Final 6. PERFORMING ORG. REPORT NUMBER
7. AUTHOR(s) Kenneth Aron and L. E. Harris		8. CONTRACT OR GRANT NUMBER(s)
9. PERFORMING ORGANIZATION NAME AND ADDRESS ARDC, LCWSL Applied Sciences Div [DRSMC-LCA-G(D)] Dover, NJ 07801		10. PROGRAM ELEMENT, PROJECT, TASK AREA & WORK UNIT NUMBERS
11. CONTROLLING OFFICE NAME AND ADDRESS ARDC, TSD STINFO Div [DRSMC-TSS(D)] Dover, NJ 07801		12. REPORT DATE November 1983 13. NUMBER OF PAGES 32
14. MONITORING AGENCY NAME & ADDRESS(If different from Controlling Office)		15. SECURITY CLASS. (of this report) UNCLASSIFIED 15a. DECLASSIFICATION/DOWNGRADING SCHEDULE
16. DISTRIBUTION STATEMENT (of this Report) Approved for public release; distribution unlimited.		
17. DISTRIBUTION STATEMENT (of the abstract entered in Block 20, if different from Report)		
18. SUPPLEMENTARY NOTES Kenneth Aron, who co-authored this report under Contract DAAK-10-81-C-0266, is associated with Geo-Centers, Inc., Newton, Massachusetts.		
19. KEY WORDS (Continue on reverse side if necessary and identify by block number) CARS Nitramine propellant RDX composite combustion Propellant decomposition		
20. ABSTRACT (Continue on reverse side if necessary and identify by block number) Coherent anti-Stokes Raman scattering (CARS) spectroscopy was used to probe the nitramine LOVA flame, burning unconfined in the air. Several spectral regions were scanned in an attempt to document the transient species of the RDX combustion for use in determining decomposition mechanisms.		

DD FORM 1 JAN 73 1473 EDITION OF 1 NOV 65 IS OBSOLETE

UNCLASSIFIED

SECURITY CLASSIFICATION OF THIS PAGE (When Data Entered)

CONTENTS

	Page
Introduction	1
Background	1
Results	2
Discussion	4
Conclusion	6
References	7
Distribution List	17

A-1

INTRODUCTION

Coherent anti-Stokes Raman scattering (CARS) spectroscopy has become one of the leading nonlinear spectroscopic techniques for non-intrusive probing of molecular species in high temperature or combustion systems (refs 1 and 2). It is particularly well suited to diagnostics in hostile environments, and is generally superior to conventional techniques since it can be used to probe systems which, like propellant flames, may be transient, incandescent, and particle-laden. To date, such systems as internal combustion engines (refs 3 and 4), jet engine after burners (ref 5), intensely sooting flames (ref 6), and gun propellant flames (ref 7) have all been probed with CARS.

The main thrust of the CARS diagnostics in those studies has been an evaluation of the post-flame zone by measurement of temperature and concentration of the equilibrium products; i.e., N_2, CO, CO_2, H_2, and H_2O. Thus, these flames have been characterized through spatial temperature and concentration mapping which has resulted in a more complete understanding of macroscopic flame phenomena. CARS capabilities can be directed towards an alternative end; that is, for use as a tool for evaluating chemical mechanisms of combustion or molecular reaction pathways. Specifically, the mechanism of a chemical reaction during combustion decomposition can be developed from information derived from CARS experimentation over a wide spectral range through the use of several laser dyes and scanning of a 1500 cm^{-1} range, the CARS spectral regions of almost every diatomic and triatomic molecule of interest in combustion reactions can be covered. In this way the transient species of the combustion decomposition reaction can be documented through a CARS probe of the reaction zone. A mechanism for RDX decomposition can, in turn, be developed--based on the transient species that can be seen with CARS and on their relative concentrations.

BACKGROUND

The theoretical background of CARS and its experimental applications have been extensively reviewed (refs 1 through 6). CARS is based on the non linear response of a homogeneous medium upon which waves ω_1 and ω_2 are incident and on an oscillating polarization generated by the response. The lowest order nonlinearity is the third order susceptibility $\chi^{(3)}(-\omega_3, \omega_1, \omega_1, -\omega_2)$ which generates a frequency component of the polarization at $\omega_3 = 2\omega_1 - \omega_2$ by the process of three wave mixing (ref 8). Vibrational resonant enhancement of this three-wave mixing process occurs if the difference between the pump laser beam (ω_1) and the Stokes laser beam (ω_2) is equal to a Raman-active vibration of the molecule

under study, thus generating the CARS signal. The observed CARS spectrum is proportional to the square of the modulus of the third order susceptibility, $\chi^{(3)}$, which is the sum of a resonant term, χ_r, related to a nuclear displacement and a non-resonant term, χ_{nr}, related to electronic displacement:

$$\chi^{(3)} = \chi_r + \chi_{nr} \tag{1}$$

χ_r is the sum of a real χ', and an imaginary component, χ'', such that,

$$(\chi^{(3)})^2 = \chi'^2 + 2\chi' \chi_{nr} + \chi''^2 + \chi_{nr}^2 \tag{2}$$

χ' and χ'' display dispersive and resonant behavior, respectively, regarding the detuning frequency, $\omega_i = \omega_j - (\omega_1 - \omega_2)$, where ω_j is the frequency of the Raman resonance. As the concentration of the resonant species is lowered, the cross term $\chi'\chi_{nr}$, which is dispersive, modulates the shape of the spectrum.

The CARS signal at $\omega_{as} = 2\omega_2 - \omega_1$ reflects the rovibrational Boltzman distribution of the molecule, from which the species temperature and concentration can be deduced. This requires a thorough knowledge of both the spectroscopic parameters of the species of interest (the contribution through χ_r) and the species composition of the gas phase, which contributes through the non-resonant susceptibility.

Since the gas composition is not known and, indeed, is one of the experimental goals, extensive iterative fitting procedures will be necessary to determine temperature and composition precisely. However, prior to full analysis, the information uncovered in this experiment (for those species seen) can be used to make qualitative and relative temperature and concentration judgments and can be related to prospective decomposition reaction mechanisms. An explanation must be made, as well, in terms of proposed mechanisms for those species for which no CARS signals were seen.

In this work, nitramine propellant was burned in open air. The nitramine propellant investigated was a CAB/NC/ATEC LOVA. Its formulation was 4% nitrocellulose, 57% RDX (NAVORDST fine grind), 19% RDX (class 5), 12% cellulose acetate butyrate, 7.6% acetyl triethyl citrate, and 0.4% ethyl centralite. The composite solid grain, a 14-mm by 14-mm cylinder of mass 3.2 gm, was probed at the surface as well as 6-mm above the surface. The CARS apparatus was identical to that reported earlier for model propellant flames (refs 9 and 10). Folded BOXCARS (ref 11), which allows for a spatial resolution of approximately 150 microns, with respect to the axis normal to the propellant surface, was carried through on both a single-shot and an averaged 10-shot basis.

RESULTS

Data from four spectral regions are shown in figures 1 through 4. A fifth region was also studied but no spectrum for this region is shown. Table 1 lists the most important combustion species predicted from nitramine decomposition, together with the theoretical or previously observed spectral frequency of the CARS signal and a summary of the observations of this work.

Briefly, CARS signals were obtained in the dark zone (the region between the nitramine surface and the beginning of the luminous zone, including the reaction zone) from CO, CO_2, H_2 (pure rotational CARS), HCN, and N_2. In addition, the CARS background modulation, typical of low concentration, was seen for NO, O_2, CH_2O), and CH_4. At a height of 6-mm above the propellant surface, only the former five species are seen.

It can empirically be stated that the dark zone, near the nitramine surface, is indeed the region being probed in this work. First, the vaporized carbohydrate matrix acts as a diluent gas, effectively creating an RDX vapor-phase solution and thereby extending the dark zone. Second, only low concentrations of N_2 and O_2 are seen at the surface in the CARS spectra, suggesting that interferences from the ambient atmosphere were small. Most important, the spectra seen at the surface for N_2, CO, and HCN all appear significantly cooler than thermochemical calculations would predict for final products (HCN is not a predicted final product). Such low temperatures--probably below 1000 K--would appear only in the dark zone near the solid surface, and not in the flame zone where the completed combustion products are present near the final flame temperature.

Figure 1, (A), shows the CARS spectrum near $\Delta\nu$ = 2100 cm^{-1} near the nitramine surface. Strong CARS signals are seen in that region from H_2 [pure rotational S-(11,9) line], CO, and HCN (ν_1), all overlapped within 100 cm^{-1}. This spectral congestion leads to extensive species-to-species interferences, severely complicating any analysis. Moreover, since the background non-resonant susceptibility is not known, a quantitative treatment cannot at this point be undertaken. It is clear from this spectrum, especially in comparison to figure 1, (B), at 6-mm height, that there exists near the solid surface, significant concentrations of H_2, CO, and HCN, all apparently below the thermochemically predicted burning temperature of 2064 K. At 6-mm height above the surface, the HCN signal has diminished, and CO and H_2 are enhanced with respect to the background. Moreover, the temperature appears hotter at this point as the CO (2,1) hot band seems to have gained intensity relative to the CO (1,0) vibrational band.

The single-shot CARS region near $\Delta\nu$ = 2350 cm^{-1} is shown in figure 2. In figure 2, (A), at the grain surface, it is apparent from the background modulation that N_2 is present at not more than a few percent concentration. The lack of any significant hot band intensity shows that the N_2 temperature is well below the equilibrium burning temperature. Figure 2, (B), at a height of 6-mm, clearly shows increased N_2 concentration and temperature, with the non-resonant background accordingly suppressed.

Several important species show CARS resonances near $\Delta\nu$ = 1500 cm^{-1} at the grain surface [fig. 3, (A)]. The H_2 S-rotational line (7,5) appears at 1446 cm^{-1}, CO_2 (ν_1 vibration) is seen at 1387 cm^{-1}, and background modulations appear from low concentrations of CH_2O (ν_3, $\Delta\nu$ = 1501 cm^{-1}), CH_4 (ν_2, $\Delta\nu$ = 1533 cm^{-1}) and O_2 ($\Delta\nu$ = 1560 cm^{-1}). In addition, the two peaks at 1406 and 1421 cm^{-1} would make an attractive HCN ($03^10\ 01^10$ and 02^00 -000 transitions, respectively)

assignment, but these transitions have been assigned at 1401 cm^{-1} and 1411 cm^{-1}, respectively (ref 12). We cannot at present account for this discrepancy. At 6-mm height, the only obvious CARS signal is the intense pure rotational H_2-S (7,5) line.

The NO CARS modulation at $\Delta\nu$ = 1876 cm^{-1} can be seen in figure 4. That this is due to a signal from a low concentration of NO is apparent by careful calibration with room temperature NO. The modulation from the H_2 (9,7) S-transition at $\Delta\nu$ = 1809 cm^{-1} is also apparent. This H_2 line dominates the spectrum at 6-mm.

Also seen in this work was a broad shoulder near $\Delta\nu$ = 1650 cm^{-1} superimposed on the background non-resonant susceptibility signal. This could possibly be correlated with the N-O stretch in RDX, or with a fragment thereof.

DISCUSSION

The above data provides the first species documentation from non-intrusive, in-situ probing of the reaction zone of RDX composite combustion. Data of this sort and data from similar CARS experiments under alternative conditions, must be included in any future modelling attempts and in evaluating existing proposed RDX combustion mechanisms. To conform to the results of this work, these mechanisms must account for initial bond breaking leading to production of relatively high concentrations of HCN near the solid surface.

In an attempt to understand the mechanisms of decomposition, extensive studies were conducted of RDX decomposition under both thermal and combustion conditions. Most data to date have been derived from thermal decomposition studies. Experiments have been conducted with isotope labeling of RDX or HMX, with mass spectrometric analysis of thermal decomposition products, and with correlations of proposed reaction pathways with observed thermodynamic quantities. What has developed from these studies is a model (ref 13) whereby the burning of composite nitramine propellants is conceptualized into two distinct vapor-phase regions, a thin near-field region and an extended far-field region. Different reactions occur in each region. The primary RDX decomposition reactions are presumed to occur in the near-field, while the reactive products generated there (such as, it is thought, CH_2O, NO_2, and N_2O) undergo further second-order reactions to complete combusiton products such as H_2O, CO, CO_2, and N_2 at final flame temperature. The heat from the near-field feeds back to drive the condensed phase processes and thus determines the burning rate. This feedback from the far-field reactions to the near-field and ultimately to the propellant surface results in a severe pressure dependence of the various reaction mechanisms.

Schroeder (ref 14) has reviewed HMX and RDX decomposition experiments and developed several critical conclusions based on thermal decomposition studies undertaken in several temperature ranges. In addition, he has discussed how decomposition mechanisms can change with changing temperature conditions, as a result of differences in activation energies of various reaction pathways. He postulates that two distinct decomposition reactions may be occurring, each with

its own temperature dependence. Specifically, at low temperatures (less than 600 K), the following gas phase reaction mechanism in which RDX initially decomposes to CH_2O + N_2O may be dominant:

$$(CH_2NNO_2)_3 \rightarrow 3CH_2O + 3N_2O \quad (3)$$

This may occur through HONO elimination and/or via the cyclic decomposition of the intermediate N-nitroformamine CH_2NNO_2.

Crossover to a high temperature reaction mechanism in the gas phase is thought to occur above about 600 K. Here cleavage of the initial N-N bond may be followed by the further decomposition of CH_2NNO_2 into H_2CN (and ultimately into HCN) and NO_2. Presumably this reaction becomes more important relative to formation of N_2O and H_2CO as the temperature rises.

Price, et al (ref 15) also draw the conclusion of increased HCN production under more extreme temperature conditions, and offer two global reactions:

$$RDX \rightarrow 4CHN + 4HNO_2 \quad (4)$$

$$RDX \rightarrow 4CHN + 4NO_2 + 2H_2 \quad (5)$$

They conclude that competing condensed phase reactions must be treated in any successful model but that HCN production should be recognized as well in any combustion model.

The data of this work support a mechanism in which HCN is produced. In addition, no significant concentrations of N_2O have been seen in this work although its CARS spectrum has previously been seen in CH_4/N_2O flames (refs 16 and 17). Its presence is predicted by many of the models in which HCN is not proposed as a product. Only a low concentration of NO is seen, and no NO_2 at all was seen in the region of the $2\nu_2$ vibration near 1500 cm^{-1}. In the NO_2 case, however, though the $2\nu_2$ CARS signal was reported (ref 18), no CARS spectrum has been obtained in our laboratory even in a bulb filled with from 50 to 500 torr NO_2. For this reason, we cannot say that no NO_2 is present in the burning propellant. NO_2 has a visible absorption which might serve to enhance an alternative multiphoton process and overwhelm CARS. Schroeder (ref 14) has pointed out that NO reacts immediately upon formation, which would also interfere with CARS detection. In summary, NO was observed at low concentration and N_2O, if produced at all, would be present only at very low concentration. No judgment concerning NO_2 can be made at this time. HCN is present in relatively high concentration near the solid surface but decreases with distance above the surface. H_2CO, CH_4, and O_2 are seen only at the solid surface (their concentrations are low). N_2 and H_2 are seen at low concentration and temperature near the propellant surface with both concentration and temperature increasing with distance above the surface. These results are consistent with mechanisms proposing HCN as a first or early product of RDX decomposition in the composite solid flame.

It should not be overlooked that most models stress the point that reaction mechanisms are highly pressure- and temperature-dependent. Whereas this experiment offers data derived from an actual combustion, these data are nonetheless

based on the moderately low pressure of 1 atmosphere. Higher pressures would compress the dark zone and make even a CARS probe substantially more difficult as a result of the spatial compression. Work is currently underway to attempt CARS measurements on propellants at higher pressures.

It is interesting to compare experimentally-derived temperature/ concentration measurements with theoretical predictions. Using the Hirschfelder thermochemical data (ref 19) on the post-flame product gases of the propellant tested, a N_2 CARS spectrum (at a height of 20-mm above the propellant surface, in the post-flame region) can be compared to the theoretical temperature 2064 K and N_2 concentration of 21.6%. Whereas this work is still being carried through and the fit shown in figure 5 needs obvious refinement, it is nonetheless evident that there is substantial agreement between the theoretically-derived and CARS-derived temperatures and concentrations.

CONCLUSION

CARS has been used to probe the dark zone of a nitramine composite propellant. Several species were seen, most notably HCN, CO, N_2, and H_2. No N_2O was seen in this work, although the CARS spectrum had been seen in model flames. These data are consistent with those models which propose HCN as a decomposition product. This information must be considered in future decomposition models.

REFERENCES

1. W. M. Tolles, J. W. Nibler, J. R. McDonald, and A. B. Harvey, Applied Spectroscopy, vol 31, 1977, p 253.

2. R. J. Hall and A. C. Eckbreth, Laser Applications, vol 5, R. K. Erf, Ed., Academic Press, New York, NY, 1982.

3. I. A. Stenhouse, D. R. Williams, J. B. Cade, and M. P. Swords, Applied Optics, vol 18, 1979, p 3819.

4. D. Klick, K. A. Marko, and L. Rimai, Applied Optics, vol 20, 1981, p 1178.

5. A. C. Eckbreth, "CARS Diagnostics for Practical Combustion Measurements," Conference on Lasers and Electro-Optics, Paper WD-1, Baltimore, MD, 1983.

6. A. C. Eckbreth, R. J. Hall, and J. A. Shirley, AIAA Paper 79-0083, 17th Aerospace Sciences Meeting, New Orleans, LA, 1979.

7. L. E. Harris and M. E. McIlwain, Combustion and Flame, vol 48 1982, p 97.

8. N. Bloembergen, Nonlinear Optics, Benjamin-Cummings, New York , 1965.

9. K. Aron, L. E. Harris, and J. Fendell, "N_2 and CO Vibration CARS and H_2 Rotational CARS Spectroscopy of CH_4-N_2O Flames," Technical Report ARLCD-TR-83033, ARRADCOM, Dover, NJ, August 1983.

10. K. Aron, L. E. Harris, and J. Fendell, Applied Optics, to be published.

11. A. C. Eckbreth, Applied Physics Letters, vol 32, 1978, p 421.

12. W. W. Brim, J. M. Hoffman, H. H. Nielsen, and K. Narahari Rao, Journal of Optical Society of America, vol 50, 1960, p 1208.

13. M. Ben Reuven and L. H. Caveny, AIAA Journal, vol 19, 1981, p 1276.

14. M. A. Schroeder, "Critical Analysis of Nitramine Decomposition Data Product Distribution from HMX and RDX," 18th JANNAF Combustion Meeting, Pasadena, CA, 1981, p 395.

15. C. F. Prince, T. L. Boggs, T. P. Parr, and D. M. Parr, 19th JANNAF Combustion Meeting, Greenbelt, MD, 1982, p 299.

16. L. E. Harris, Chemical Physics Letters, vol 93, 1982, p 335.

17. L. E. Harris, Combustion and Flame, to be published.

18. D. M. Grothals, K. P. Cross, and J. W. Nibler, Journal of Chemical Physics, vol 70, 1979, p 2393.

19. J. O. Hirschfelder, R. B. Kershner, and C. F. Curtiss, "Interim Ballistics I," Report A-142, National Defense Research Commission, 1943.

Table 1. Species of interest in nitramine decomposition

Species	Standard Raman frequency (cm^{-1})[a,b]	Comments
N_2	2330	Low concentration observed at surface
N_2O (ν_1)	2223	Not observed in this work
CO	2137	Strong CARS signal at surface
H_2 (S-11,9)	2131[c]	Strong CARS signal
HCN (ν_1)	2087	Strong signal diminishes with probe height
NO	1876	Low concentration modulation observed
H_2 (S-9,7)	1809[d]	Strong CARS signal at 6-mm height
O_2	1556	Low concentration modulation observed[e]
CH_4 (ν_2)	1533	Low concentration modulation observed
CH_2O (ν_3)	1503	Low concentration modulation observed
NO_2 ($2\nu_2$)	1500	Not observed in this work
H_2 (S-7,5)	1446[f]	Strong CARS signal
HCN (02^00-000)	1411	Moderately strong at surface[e]
HCN (03^10-01^10)	1401	Moderately strong at surface[e]
CO_2 (ν_1)	1388	Moderately strong at surface

---

a G. H. Herzberg, Spectra of Diatomic Molecules, second edition, Van Nostrand Reinhold, New York, NY, 1950.

b G. H. Herzberg, Infrared and Raman Spectra, Van Nostrand Reinhold, New York, NY, 1945.

c R. Farrow, P. Mattern, and L. A. Rahn, 7th International Raman Conference, 1980, p 668.

d K. Aron, L. E. Harris, and J. Fendell, Applied Optics, to be published.

e Observed frequency in this work differs by more than 5 cm^{-1} with standard frequencies.

f Based on constants of V. Fink, T. A. Wiggins, and D. H. Rank, Journal of Molecular Spectroscopy, vol 18, 1965, p 384.

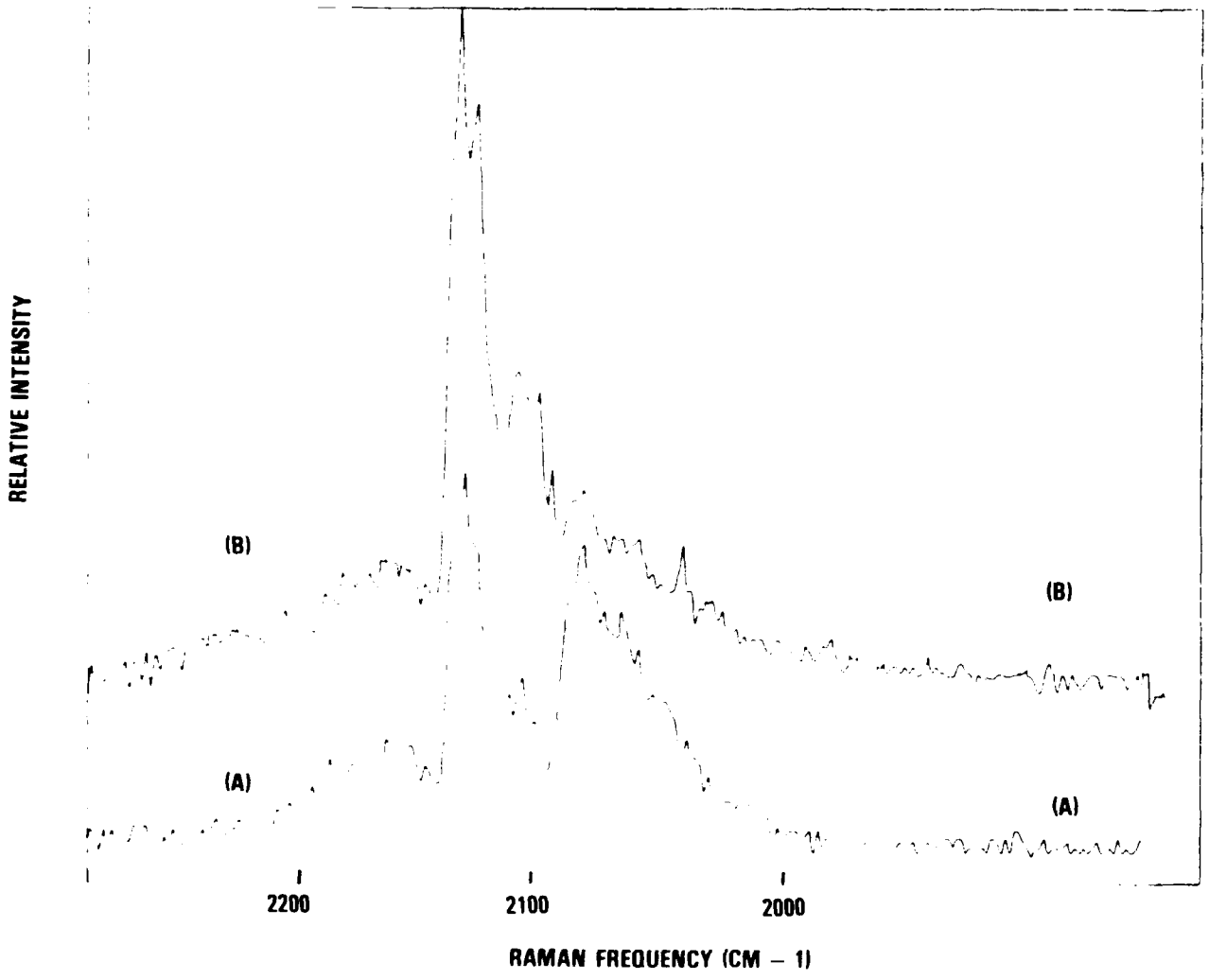

Figure 1. (A) The single-shot CARS spectrum at the nitramine surface and (B) the averaged CARS spectrum at a height of 6-mm above the nitramine surface in the region ν = 2100 cm^{-1}. At the surface, strong signals are seen from H_2, CO, and HCN whereas the HCN signal is diminished at 6-mm with respect to the CO or H_2.

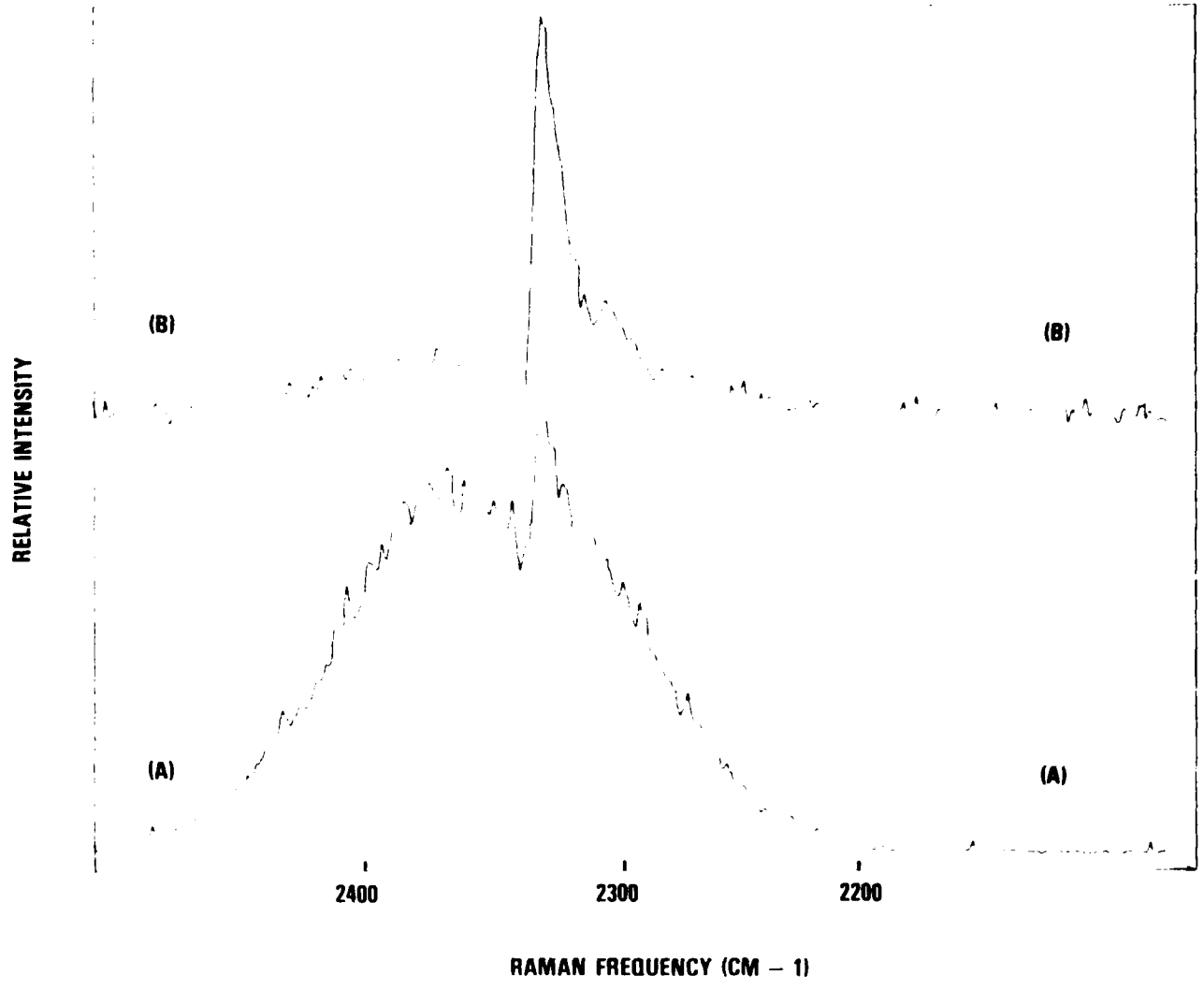

Figure 2. (A) The single-shot CARS spectrum at the nitramine surface and (B) the averaged CARS spectrum at a height of 6-mm above the nitramine surface in the region $\Delta\nu$ = 2300 cm^{-1}. At the surface, the low concentration N_2 signal is superimposed on the non-resonant background, but the N_2 signal increases as the probe position is raised.

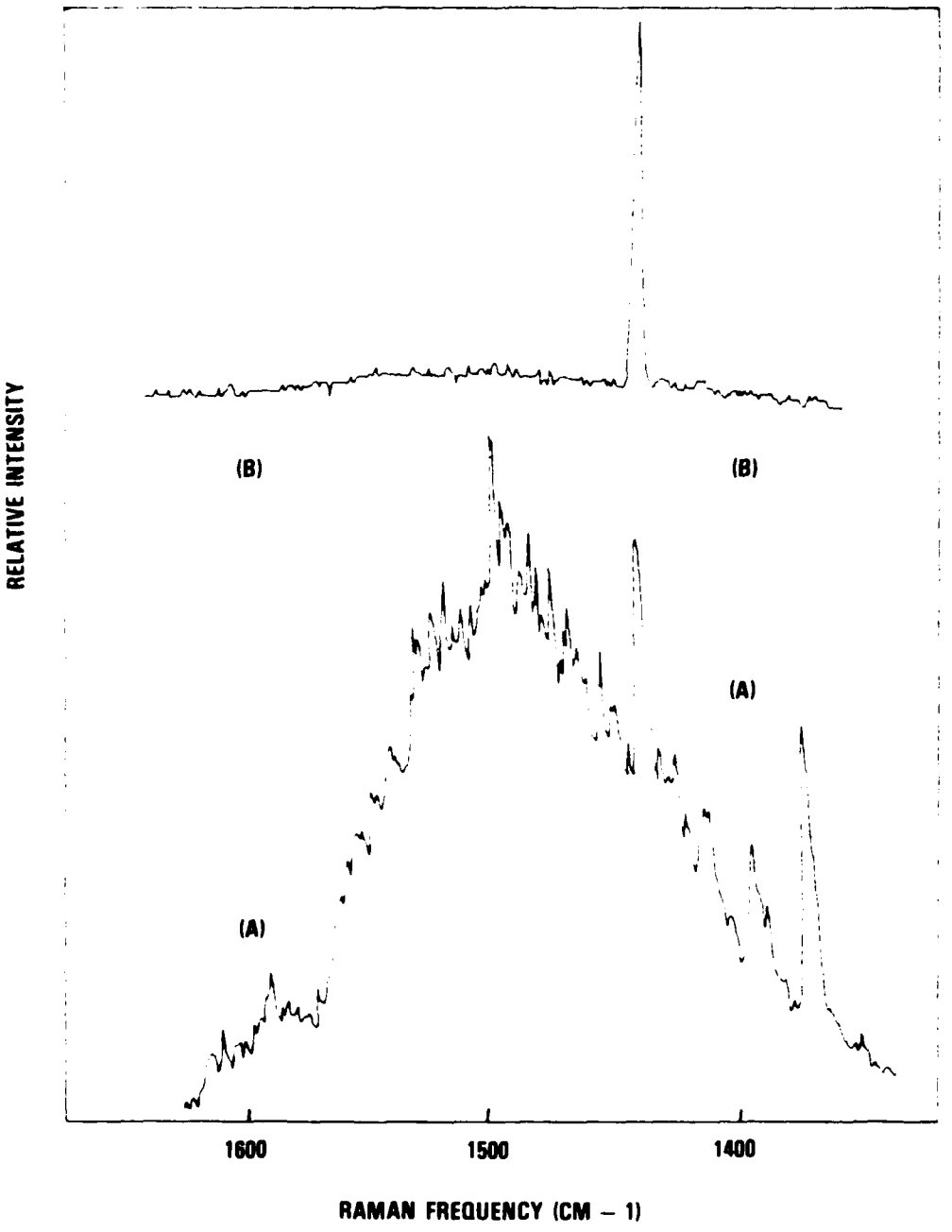

Figure 3. (A) The single-shot CARS spectrum at the nitramine surface and (B) the averaged CARS spectrum at a height of 6-mm above the nitramine surface at the region $\Delta\nu$ = 1500 cm^{-1}. Superimposed on the non-resonant background are CARS signals from CO_2, HCN, H_2, CH_2O, CH_4, and O_2. As the probe height is raised, only the pure rotational H_2 CARS signal is apparent.

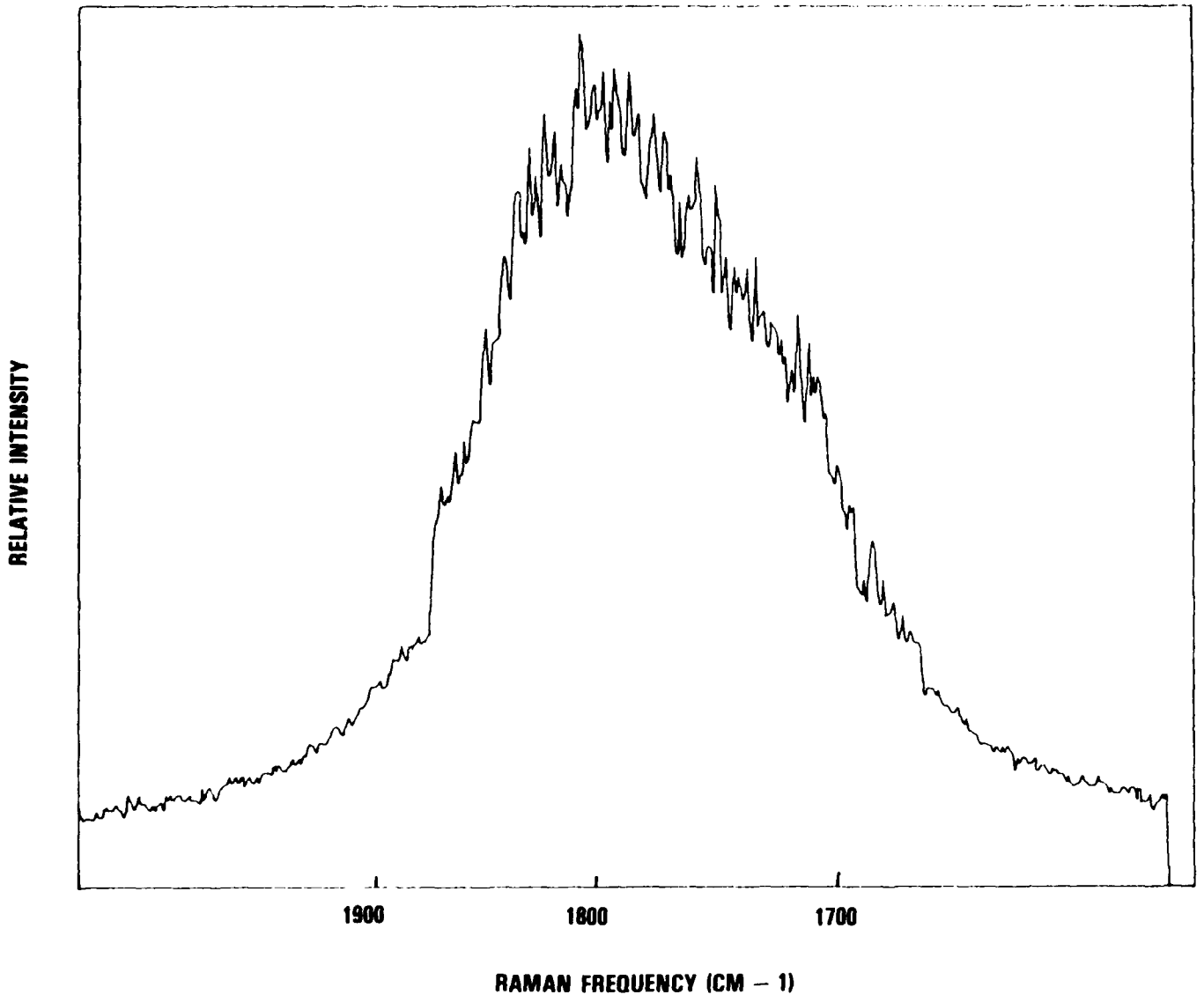

Figure 4. The CARS signal in the $\Delta\nu$ = 1750 cm^{-1} region at the nitramine surface. A background modulation due to NO is apparent near 1876 cm^{-1}.

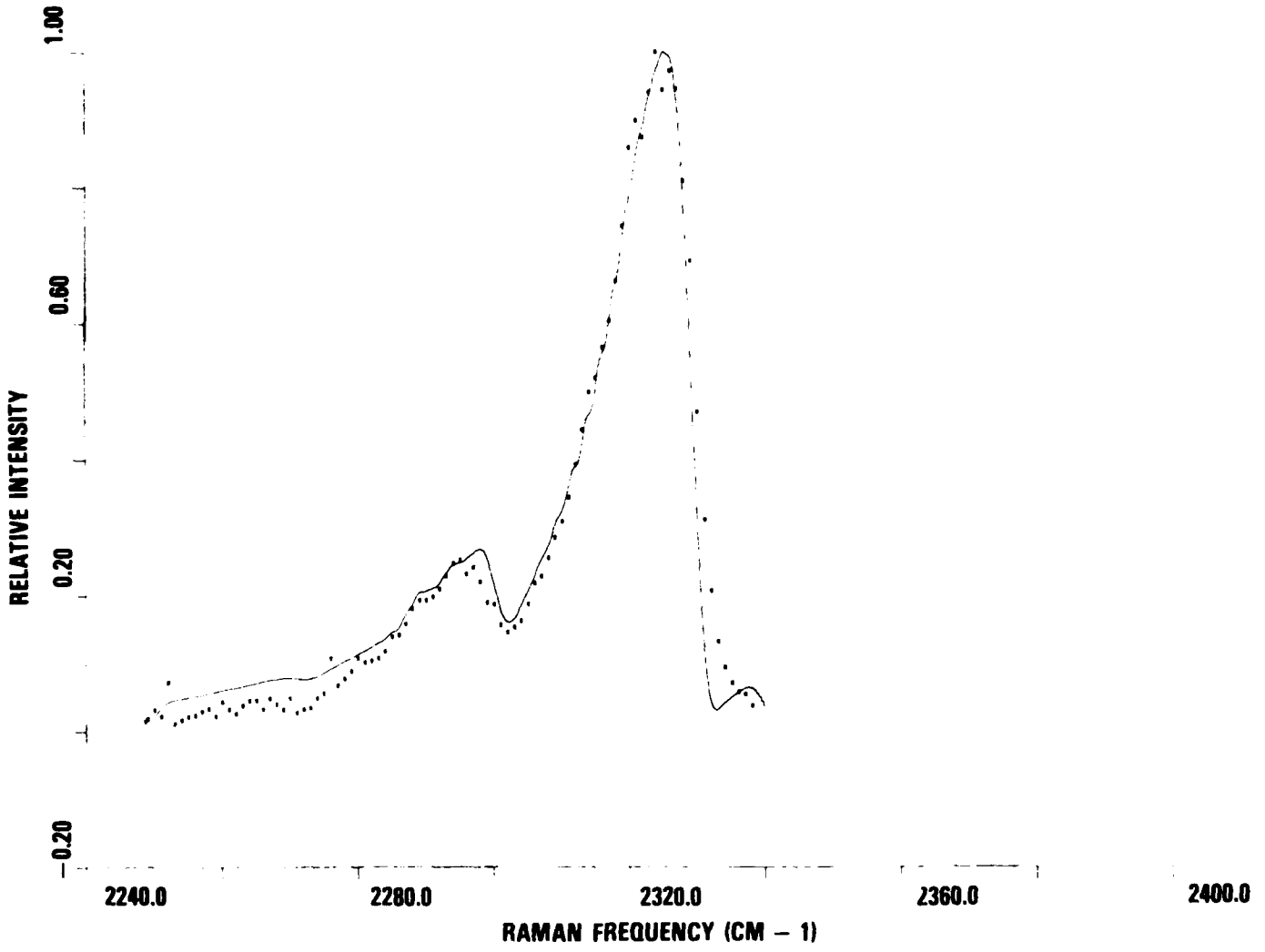

Figure 5. N_2 CARS spectrum of LOVA nitramine propellant at a height of 20-mm above the propellant surface. The dots represent the experimental points while the solid line is the computed spectrum using the Hirschfelder values of temperature (2064 K) and N_2 concentration (21.6%) and species composition of post-flame gas.

DISTRIBUTION LIST

Commander
Armament Research and Development Center
U.S. Army Armament, Munitions and
Chemical Command
ATTN: DRSMC-TSS(D) (5)
DRSMC-TDC(D), D. A. Gyorog
DRSMC-GCL(D)
DRSMC-LC(D), J. Frasier
J. P. Picard
DRSMC-LCA(D), T. Davidson
DRSMC-LCA-G(D), J. Lannon
D. Downs
L. Harris (10)
T. Vladimiroff
A. Beardell
Y. Carignon
J. Fendell
K. Aron (10)
E. Petro
DRSMC-LCE(D), R. Walker
P. Marinkas
C. Capellos
F. Owens
S. Bulusu
F. Gilbert
Dover, NJ 07801

Administrator
Defense Technical Information Center
ATTN: Accessions Division (12)
Cameron Station
Alexandria, VA 22314

Director
U.S. Army Materiel Systems
Analysis Activity
ATTN: DRXSY-MP
Aberdeen Proving Ground, MD 21005

Commander
Chemical Research and Development Center
U.S. Army Armament, Munitions and
Chemical Command
ATTN: DRSMC-CLJ-L(A)
DRSMC-CLB-PA(A)
APG, Edgewood Area, MD 21010

Director
Ballistics Research Laboratory
Armament Research and Development Center
U.S. Army Armament, Munitions and
Chemical Command
ATTN: DRSMC-TSB-S(A)
DRSMC-BLP(A), L. Watermier
A. Barrows
G. Adams
R. Fifer
M. Miller
T. Coffee
J. Heimeryl
C. Nelson
J. Vanderhoff
J. Anderson
Aberdeen Proving Ground, MD 21005

Chief
Benet Weapons Laboratory, LCWSL
Armament Research and Development Center
U.S. Army Armament, Munitions and
Chemical Command
ATTN: DRSMC-LCB-TL
Watervliet, NY 12189

Commander
U.S. Army Armament, Munitions and
Chemical Command
ATTN: DRSMC-LEP-L(R)
Rock Island, IL 61299

Director
U.S. Army TRADOC Systems
Analysis Activity
ATTN: ATAA-SL
White Sands Missile Range, NM 88002

Director
Defense Advanced Research Projects
Agency
ATTN: LTC C. Buck
1400 Wilson Boulevard
Arlington, VA 22209

Commander
U.S. Army Materiel Development
and Readiness Command
ATTN: DRCDMD-ST
5001 Eisenhower Avenue
Alexandria, VA 22333

Commander
U.S. Army Watervliet Arsenal
ATTN: SARWV-RD, R. Thierry
Watervliet, NY 12189

Director
U.S. Army Air Mobility Research
and Development Laboratory
Ames Research Center
Moffett Field, CA 94035

Commander
U.S. Army Communications Research
and Development Command
ATTN: DRDCO-PPA-SA
Fort Monmouth, NJ 07703

Commander
U.S. Army Electronics Research
and Development Command
Technical Support Activity
ATTN: DELSD-L
Fort Monmouth, NJ 07703

Commander
U.S. Army Missile Command
ATTN: DRSMI-R
DRSMI-YDL
Redstone Arsenal, AL 35809

Commander
U.S. Army Natick Research
and Development Command
ATTN: DRXRE, D. Sieling
Natick, MA 01762

Commander
U.S. Army Tank Automotive Research
and Development Command
ATTN: DRDTA-UL
Warren, MI 48090

Commander
U.S. Army White Sands Missile Range
ATTN: STEWS-VT
White Sands Missile Range, NM 88002

Commander
U.S. Army Materials and
Mechanics Research Center
ATTN: DRXMR-ATL
Watertown, MA 02172

Commander
U.S. Army Research Office
ATTN: Technical Library
D. Squire
F. Schmiedeshaff
R. Ghirardelli
M. Ciftan
P.O. Box 12211
Research Triangle Park, NC 27706

Office of Naval Research
ATTN: Code 473
G. Neece
800 N. Quincy Street
Arlington, VA 22217

Commander
Naval Sea Systems Command
ATTN: J. W. Murrin, SEA-62R2
National Center
Bldg 2, Room 6E08
Washington, DC 20362

Commander
Naval Surface Weapons Center
ATTN: Library Branch, DX-21
Dahlgren, VA 22448

Commander
Naval Surface Weapons Center
ATTN: Code 240, S. J. Jacobs, J. Sharma
Code 730
Silver Spring, MD 20910

Commander
Naval Underwater Systems Center
Energy Conversion Department
ATTN: Code 5B331, R. S. Lazar
Newport, RI 02840

Commander
Naval Weapons Center
ATTN: R. Derr
C. Thelen
China Lake, CA 93555

Commander
Naval Research Laboratory
ATTN: Code 6180
Washington, DC 20375

Superintendent
Naval Postgraduate School
ATTN: Technical Library
D. Netzer
A. Fuhs
Monterey, CA 93940

Commander
Naval Ordnance Station
ATTN: Dr. Charles Dale
Technical Library
Indian Head, MD 20640

AFOSR
ATTN: J. F. Masi
B. T. Wolfson
D. Ball
L. Caveny
Bolling AFB, DC 20332

AFRPL (DYSC)
ATTN: D. George
J. N. Levine
Edwards AFB, CA 93523

National Bureau of Standards
ATTN: J. Hastie
T. Kashiwagi
H. Semerjian
M. Jacox
K. Smyth
J. Stevenson
Washington, DC 20234

Lockheed Palo Alto Research Laboratories
ATTN: Technical Information Center
3521 Hanover Street
Palo Alto, CA 94304

Aerojet Solid Propulsion Co.
ATTN: P. Micheli
Sacramento, CA 95813

ARO Incorporated
ATTN: N. Dougherty
Arnold AFS, TN 37389

Atlantic Research Corporation
ATTN: M. K. King
5390 Cherokee Avenue
Alexandria, VA 22314

AVCO Corporation
AVCO Everett Research Laboratory
Division
ATTN: D. Stickler
2385 Revere Beach Parkway
Everett, MA 02149

Calspan Corporation
ATTN: E. B. Fisher
A. P. Trippe
P.O. Box 400
Buffalo, NY 14221

Foster Miller Associates, Inc.
ATTN: A. J. Erickson
135 Second Avenue
Waltham, MA 02154

General Electric Company
Armament Department
ATTN: M. J. Bulman
Lakeside Avenue
Burlington, VT 05402

General Electric Company
Flight Propulsion Division
ATTN: Technical Library
Cincinnati, OH 45215

Hercules Incorporated
Alleghany Ballistic Lab
ATTN: R. Miller
Technical Library
Cumberland, MD 21501

Hercules Incorporated
Bacchus Works
ATTN: B. Isom
Magna, UT 84044

IITRI
ATTN: M. J. Klein
10 West 35th Street
Chicago, IL 60615

Olin Corporation
Badger Army Ammunition Plant
ATTN: J. Ramnarace
Baraboo, WI 53913

Olin Corporation
New Haven Plant
ATTN: R. L. Cook
D. W. Riefler
275 Winchester Avenue
New Haven, CT 06504

Paul Gough Associates, Inc.
ATTN: P. S. Gough
P.O. Box 1614
Portsmouth, NH 03801

Physics International Company
2700 Merced Street
Leandro, CA 94577

Pulsepower Systems, Inc.
ATTN: L. C. Elmore
815 American Street
San Carlos, CA 94070

Rockwell International Corp.
Rocketdyne Division
ATTN: C. Obert
J. E. Flanagan
A. Axeworthy
6633 Canoga Avenue
Canoga Park, CA 91304

Rockwell International Corp.
Rocketdyne Division
ATTN: W. Haymes
Technical Library
McGregor, TX 76657

Science Applications, Inc.
ATTN: R. B. Edelman
Combustion Dynamics and
Propulsion Division
23146 Cumorah Crest
Woodland Hills, CA 91364

Shock Hydrodynamics, Inc.
ATTN: W. H. Anderson
4710-16 Vineland Avenue
N. Hollywood, CA 91602

Thiokol Corporation
Elkton Division
ATTN: E. Sutton
Elkton, MD 21921

Thiokol Corporation
Huntsville Division
ATTN: D. Flanigan
R. Glick
Technical Library
Huntsville, AL 35807

Thiokol Corporation
Wasatch Division
ATTN: J. Peterson
Technical Library
P.O. Box 524
Brigham City, UT 84302

TRW Systems Group
ATTN: H. Korman
One Space Park
Redondo Beach, CA 90278

United Technologies
Chemical Systems Division
ATTN: R. Brown
Technical Library
P.O. Box 358
Sunnyvale, CA 94086

Battelle Memorial Institute
ATTN: Technical Library
R. Bartlett
505 King Avenue
Columbus, OH 43201

Brigham Young University
Department of Chemical Engineering
ATTN: M. W. Beckstead
Provo, UT 84601

California Institute of Technology
204 Karmar Lab
Mail Stop 301-46
ATTN: F. E. C. Culick
1201 E. California Street
Pasadena, CA 91125

Case Western Reserve University
Division of Aerospace Sciences
ATTN: J. Tien
Cleveland, OH 44135

Georgia Institute of Technology
School of Aerospace Engineering
ATTN: B. T. Zinn
E. Price
W. C. Strahle
Atlanta, GA 30332

Institute of Gas Technology
ATTN: D. Gidaspow
3424 S. State Street
Chicago, IL 60616

Johns Hopkins University/APL
Chemical Propulsion Information Agency
ATTN: T. Christian
Johns Hopkins Road
Laurel, MD 20810

Massachusetts Institute of Technology
Department of Mechanical Engineering
ATTN: T. Toong
Cambridge, MA 02139

Pennsylvania State University
Applied Research Laboratory
ATTN: G. M. Faeth
P.O. Box 30
State College, PA 16801

Pennsylvania State University
Department of Mechanical Engineering
ATTN: K. Kuo
University Park, PA 16801

Pennsylvania State University
Department of Material Sciences
ATTN: H. Palmer
University Park, PA 16801

Princeton Combustion Research
Laboratories
ATTN: M. Summerfield
N. Messina
1041 U.S. Highway One North
Princeton, NJ 08540

Princeton University
Forrestal Campus
ATTN: I. Glassman
F. Dryer
Technical Library
P.O. Box 710
Princeton, NJ 08540

Purdue University
School of Mechanical Engineering
ATTN: J. Osborn
S. N. B. Murthy
N. M. Laurendeau
TSPC Chaffee Hall
W. Lafayette, IN 47906

Rutgers State University
Department of Mechanical and
Aerospace Engineering
ATTN: S. Temkin
University Heights Campus
New Brunswick, NJ 08903

SRI International
ATTN: Technical Library
D. Crosley
J. Barker
D. Golden
333 Ravenswood Avenue
Menlo Park, CA 94025

Stevens Institute of Technology
Davidson Library
ATTN: R. McAlevy, III
Hoboken, NJ 07030

United Technology
ATTN: Alan Eebreth
Robert Hall
Research Center
East Hartford, CT 06108

Commander
Naval Research Laboratory
Chemistry Division
ATTN: A. Harvey
Washington, DC 20375

General Motors Research Laboratory
ATTN: J. H. Bechtel
Warren, Michigan 48090

System Research Laboratory
ATTN: L. Goss
2600 Indian Ripple Rd
Dayton, Ohio 45440

Exxon Research and Engineering
ATTN: A. Dean
M. Chou
P.O. Box 45
Linden, NJ 07036

Ford Motor Company
Research Staff
ATTN: K. Marko
L. Rimai
Dearborn, Michigan 48120

Sandia Laboratories
Applied Physics Division I
ATTN: L. Rahn
D. Stephenson
Livermore, CA 94550

Rensselaer Polytechnic Institute
Dept. of Chem. Engineering
ATTN: A. Fontijn
Troy, NY 12181

University of California,
San Diego
Ames Department
ATTN: F. Williams
P.O. Box 109
La Jolla, CA 92037

University of California
Dept. of Mechanical Eng.
ATTN: J. W. Daily
Berkeley, CA 94720

University of Dayton
University of Dayton Research Inst.
Dayton, OH 45406

University of Florida
Dept. of Chemistry
ATTN: J. Winefordner
Gainesville, Florida 32601

University of Illinois
Dept. of Mechanical Eng.
ATTN: H. Krier
144 MEB, 1206 W. Green St.
Urbana, IL 61801

University of Minnesota
Dept. of Mechanical Eng.
ATTN: E. Fletcher
Minneapolis, MN 55455

University of California,
Santa Barbara
Quantum Institute
ATTN: K. Schofield
M. Steinberg
Santa Barbara, CA 93106

University of Southern California
Department of Chemistry
ATTN: S. Benson
Los Angeles, CA 90007

Stanford University
Department of Mech. Eng.
ATTN: R. Hanson
Stanford, CA 93106

University of Texas
Department of Chemistry
ATTN: W. Gardiner
H. Schaefer
Austin, TX 78712

University of Utah
Dept. of Chemical Engineering
ATTN: A. Baer
G. Flandro
Salt Lake City, UT 84112